Relativistic calculations for Fe XXIII: Electron-impact excitation

Chen Guo-xin and P. P. Ong
Physics Department, National University of Singapore, Singapore 119260
(Received 9 December 1997)

Relativistic distorted-wave method was used to calculate the electron-impact excitation processes for Fe XXIII. Collision strengths for the resonant transitions and transitions between excited levels within the first 46 levels of Fe XXIII are reported. Multiconfiguration Dirac-Fock wave functions with 133-level configuration expansion were used to describe the target-ion states accurately. The distorted-wave potentials with semiclassical exchange potential were used to determine the continuum orbitals. The collision strengths for some of the transitions in $n=2-3$ were previously calculated only by a nonrelativistic distorted-wave method. If they are compared with our results, significant differences are found. The reason for these differences is explained. The accuracy of the collision strength for the transition from the ground state to $2s2p\ ^3P_1$ is reestimated among different methods. Because of the accurate target states used and the fully relativistic effect caught in the atomic structure and relativistic distorted-wave method used in the collision dynamics, the collision strengths provided in the present calculation should be accurate and reliable. Also, we report collision strengths for some of the $n=3-3$ transitions in this paper. These electron impact excitation results have various applications in solar flare spectra, plasma modeling and diagnostics, and in achieving population inversion in the development of x-ray lasers. [S1050-2947(98)03708-1]

PACS number(s): 34.50.Fa, 02.70.−c, 34.80.Kw

I. INTRODUCTION

Accurate excitation collision strengths of Fe XXIII by electron impact are very necessary for the UV and x-ray lines modeling in solar flare and various kinds of plasmas produced in astrophysics and the laboratory [1,2]. Electron-impact excitation (EIE) is one of the most important mechanisms to generate population inversion needed in the design of UV or x-ray lasers. To get accurate collision strengths, both atomic structure and collision dynamics must be suitably described. The relativistic effect begins to demonstrate a great influence on the atomic structure and collision dynamics for Fe XXIII in contrast to lower Z Be-like ions. The atomic structure of Fe XXIII has been accurately calculated in a contemporary paper of ours [3], where the relativistic effect was caught by Dirac-Coulomb Hamiltonian H^{DC} and most of the important correlation effect was caught by large-scale multiconfiguration Dirac-Fock (MCDF) configuration expansion (CE). Also, higher-order relativistic effects were perturbatively included. Relativistic effects in collision dynamics are also very important. These effects come from the relativistic kinematics of free electrons and relativistic Møller electron-electron scattering between bound and free electrons [4]. Although Møller interaction is not important for Fe XXIII because not very high incident electron energy is involved, it is important to use relativistic continuum orbitals.

The present electron-impact excitation calculations are extensively compared with other results, wherever available. Most of the previous calculations were for collision strengths of the $n=2-2$ transitions. Norrington and Grant calculated transitions within the first ten levels by using a Dirac R-matrix code [5,6], whereas one transition from the ground state $2s^2\ ^1S_0$ to $2s2p\ ^3P_1$ has been obtained by the Breit-Pauli R-matrix method [7]. Also, fully relativistic distorted-wave (RDW) collision strengths among the first ten levels were obtained by Zhang and Sampson [8,9]. Certain $n=2-2$ transitions were also obtained by Qian *et al.* by using their RDW code [10]. It is more complicated to calculate the collision strengths for $n=2-3$ transitions because they are more sensitive to both bound and free orbitals, electron correlation, relativistic effects, models used such as the size of configuration expansion, and so on. However, no results have appeared in the literature using the very accurate Dirac R-matrix method, nonrelativistic with the Breit-Pauli R-matrix method, or fully RDW method. EIE of certain $n=2-3$ transitions from levels in $2s^2,2p^2$ to levels in $2s3p,2p3s,2p3d$ have been calculated by the nonrelativistic Coulomb-Born exchange method [11]. Rather extensive $n=2-3$ transitions from levels in $2s^2,2s2p$ to levels in $2s3s,2s3p,2s3d$ have been calculated by a nonrelativistic distorted-wave (DW) code [12–14] with some of the relativistic corrections by Bhatia and Mason [15,16].

In this paper, more comprehensive calculations than before were carried out by fully RDW method. The transitions included are both those among the first ten levels and those from levels in $2s^2,2s2p,2p^2,2s3l$ $(l=s,p,d)$ to levels in $2s3l,2p3l$ $(l=s,p,d)$. Also, the 133-level CE, which can be seen in [3], has been used in obtaining the atomic structure assumed in these EIE calculations. Comparisons for these calculations are made and the accuracies of the collision strengths by different methods are estimated. Especially, it is found that the number of partial waves used in the relativistic R-matrix [5,6], nonrelativistic R-matrix [7], and nonrelativistic DW calculations [15,16] may not be large enough to evaluate the collision strength (CS) for transition from $2s^2\ ^1S_0$ to $2s2p^3\ P_1$. Large differences occur between these calculations and ours. Our result for this transition agrees better with those in Refs. [5–7] than those in Refs. [10,15,16].

In Sec. II the theory of RDW EIE is briefly outlined. The generalized occupation numbers were used to determine the

distorted potentials. The collision strengths of EIE for Fe XXIII are presented in Sec. III. Comparisons with other calculations are made in tables or figures. Also, detailed discussions for these comparisons are given in this section. Finally, we present a summary and conclusion in Sec. IV.

II. OUTLINE OF RDW COLLISION THEORY

The RDW procedures used in the present calculations are given in Ref. [17]. Here, we only restate some main points to establish convention and notion. It is convenient to express the relativistic cross section $\sigma_{if}(\epsilon)$ for the transition $i \rightarrow f$ in terms of collision strength $\Omega_{if}(\epsilon)$ by the relation

$$\sigma_{if}(\epsilon) = \frac{\pi a_0^2}{k_i^2 g_i} \Omega_{if}(\epsilon), \tag{2.1}$$

where the subscripts i and f refer to the initial and final states, a_0 is Bohr radius, k_i is the relativistic wave number of the impact electron, $g_i = [J_i] = 2J_i + 1$ is the statistical weight of the initial state of the N-electron target ion. The relation between the relativistic wave quantum number k of the impact electron and its relativistic momentum p and kinetic energy ϵ (in a.u.) is

$$k^2 = \frac{p^2 a_0^2}{\hbar^2} = \epsilon \left[2 + \frac{\epsilon}{c^2} \right]. \tag{2.2}$$

c is the light speed in a.u. The total collision strength is computed by summing over the partial collision strengths, which are computed from the transition matrix T. T can be expressed in terms of reactance matrix K. For highly charged ions of interest here, the elements of K are small, so that weak-coupling approximation made in RDW method gives a good treatment. Then, the collision strength Ω_{if} can be obtained by [9]

$$\Omega_{if} = 8 \sum BQ, \tag{2.3}$$

where sums are over all the target configuration state functions (CSF) included and the rank of C tensor in angular part. B in Eq. (2.3) depends only on the properties of the target. Q in Eq. (2.3) contains the radial scattering matrix elements and have the summation over initial and final orbitals and total angular momenta of the free electron performed within them. Therefore, Eq. (2.3) can be called the factorization form of RDW theory, which enables fast calculations for EIE.

The direct part of distorted potentials $V'(r)$ in a.u. for calculating the continuum orbitals are the spherically averaged potentials of the nucleus plus the bound electrons in the bound state. The exchange potentials $V^{\mathrm{ex}}(r)$ are chosen to be the semiclassical exchange (SCE) approximation [9,17], which are local energy-dependent exchange potentials,

$$V^{\mathrm{ex}}(r) = \frac{1}{2} [V'(r) - \epsilon] [(1 + \beta^2)^{1/2} - 1], \tag{2.4}$$

where

$$\beta^2 = \frac{4\pi\rho(r)}{[V'(r) - \epsilon]^2}, \tag{2.5}$$

Here, ϵ is the free-electron kinetic energy in atomic units. The potentials used in calculating the orbitals of the impact and scattered electrons for a certain transition differed only by different free-electron energies. Finite nuclear charge $Z(r)$, which differs from ordinary Z only for small r, is chosen to be the Fermi charge distribution and can be obtained from GRASP[2] code [18,19]. To make our RDW calculation physically more plausible and consistent with the given atomic structure, in contrast to previous calculations, $\overline{q}(a)$ determined in Eq. (2.4) of Ref. [3] and given in Table II of Ref. [3] replaces $\omega_{n'\kappa'}$ in Eqs. (22) and (23) of Ref. [17] or Eqs. (23) and (24) of Ref. [9] in the present calculations. $\omega_{n'\kappa'}$ were previously chosen by assuming fictitious occupation numbers extensively, e.g., Eq. (28) of Ref. [17] or Eq. (1) of Ref. [9], whereas in our present calculations $\overline{q}(a)$ are directly determined from MCDF self-consistent-field (SCF), which allows them to be readjusted according to the mixing coefficients. Hence the latter procedure should be physically more reasonable in determining the distorted potentials in our RDW calculations. Application of this new distorted potential caused the calculated collision strengths to change by a few percent [20]. In the above-mentioned choice of potential, since the orbitals of the free electron so calculated are not orthogonal to those of the bound electrons, it is necessary to make some modifications in calculating the exchange matrix elements of the reaction matrix.

III. NUMERICAL CALCULATION OF COLLISION STRENGTHS AND DISCUSSIONS

In Table I we tabulate the collision strengths at eight electron impact energies E_i for resonance transitions to levels in the $n=2$ complex. The level indices have been given elsewhere [3]. Both results with the 133-level MCDF configuration-expansion (CE) and the 20-level MCDF CE (see Ref. [3]) of the present RDW calculation are included in the first and second entries for each transition, respectively. Also, collision strengths by nonrelativistic DW plus relativistic correction and intermediate coupling in the 46-level CE calculated by Bhatia and Mason [16] are listed in the third entries; some results at selected electron-impact energies calculated by the Dirac R-matrix method for transition 1–3 [5], by RDW method for transitions 1–3 and 1–5 by Qian *et al.* [10], and by RDW method for transitions 1–9 and 1–10 by Zhang and Sampson [8] are given in the fourth entries for comparisons. The results in the second entries are generally in good agreement within 3% with those in the first entries for each transition in Table I. This indicates that most of the correlation effects are caught in the 20-level MCDF CE for the calculations of the resonant excitation transitions in the $n=2$ complex. Also, the present results for transitions 1–3 and 1–5 are in good agreement with those calculated by Qian *et al.* [10]. When comparisons between the first or second entries and the third entries for each transition are made at high impact energies, the discrepancies for half of the transitions are less than 10%. However, large discrepancies for the other transitions, i.e., 10% for 1–3, 32% for 1–6,

TABLE I. Comparison of collision strengths for resonance transitions at different E_i to levels in the $n=2$ complex. For each transition, the first and second entries were calculated by the present approach using the 133- and 20-level MCDF configuration expansion, respectively, while the third entries were nonrelativistic results by Bhatia and Mason [16]. Some other calculations are given in the fourth entries as footnoted. The level indices for transition are given under the heading levels: I and F, where I stands for the initial level and F the final level.

Transition	E_i (Ry)							
$I-F$	15.0	30.0	45.0	85.0	127.5	170.0	250.0	350.0
1–2	1.24[−3][a]	1.10[−3]	9.72[−4]	7.17[−4]	5.38[−4]	4.18[−4]	2.79[−4]	1.85[−4]
	1.28[−3]	1.13[−3]	9.98[−4]	7.33[−4]	5.49[−4]	4.25[−4]	2.83[−4]	1.87[−4]
	1.33[−3]	1.17[−3]	1.03[−3]	7.48[−4]	5.61[−4]	4.31[−4]	2.83[−4]	1.85[−4]
1–3	1.07[−2]	1.12[−2]	1.18[−2]	1.25[−2]	1.31[−2]	1.34[−2]	1.43[−2]	1.49[−2]
	1.07[−2]	1.14[−2]	1.22[−2]	1.27[−2]	1.32[−2]	1.33[−2]	1.43[−2]	1.47[−2]
	1.23[−2]	1.24[−2]	1.25[−2]	1.22[−2]	1.24[−2]	1.26[−2]	1.30[−2]	1.35[−2]
	8.6[−3][b]		1.17[−2][c]	1.23[−2][c]				1.40[−2][c]
1–4	6.10[−3]	5.38[−3]	4.75[−3]	3.49[−3]	2.61[−3]	2.02[−3]	1.34[−3]	8.85[−4]
	6.29[−3]	5.54[−3]	4.88[−3]	3.56[−3]	2.66[−3]	2.05[−3]	1.36[−3]	8.94[−4]
	6.34[−3]	5.56[−3]	4.90[−3]	3.61[−3]	2.67[−3]	2.05[−3]	1.35[−3]	8.79[−4]
1–5	3.15[−1]	3.41[−1]	3.64[−1]	4.18[−1]	4.68[−1]	4.95[−1]	5.48[−1]	5.87[−1]
	3.08[−1]	3.30[−1]	3.56[−1]	4.14[−1]	4.73[−1]	4.99[−1]	5.57[−1]	5.92[−1]
	2.74[−1]	3.07[−1]	3.36[−1]	3.95[−1]	4.35[−1]	4.69[−1]	5.14[−1]	5.55[−1]
			3.59[−1][c]	4.10[−1][c]				5.70[−1][c]
1–6	1.28[−4]	1.17[−4]	1.09[−4]	9.37[−5]	8.54[−5]	8.03[−5]	7.43[−5]	7.41[−5]
	1.27[−4]	1.15[−4]	1.06[−4]	9.01[−5]	8.07[−5]	7.51[−5]	6.90[−5]	6.67[−5]
	1.16[−4]	1.05[−4]	0.97[−4]	0.81[−4]	0.73[−4]	0.66[−4]	0.60[−4]	0.56[−4]
1–7	1.62[−4]	1.33[−4]	1.11[−4]	7..16[−5]	4.82[−5]	3.41[−5]	1.97[−5]	1.13[−5]
	1.70[−4]	1.39[−4]	1.15[−4]	7.40[−5]	4.95[−5]	3.50[−5]	2.01[−5]	1.14[−5]
	1.50[−4]	1.25[−4]	1.05[−4]	0.68[−4]	0.47[−4]	0.33[−4]	0.19[−4]	0.11[−4]
1–8	5.05[−4]	4.92[−4]	4.82[−4]	4.69[−4]	4.66[−4]	4.69[−4]	4.76[−4]	4.87[−4]
	5.03[−4]	4.88[−4]	4.76[−4]	4.60[−4]	4.57[−4]	4.59[−4]	4.66[−4]	4.76[−4]
	5.35[−4]	4.97[−4]	4.72[−4]	4.23[−4]	4.03[−4]	3.87[−4]	3.65[−4]	3.41[−4]
1–9	8.07[−4]	8.48[−4]	8.80[−4]	9.45[−4]	9.96[−4]	1.03[−3]	1.09[−3]	1.13[−3]
	7.86[−4]	8.25[−4]	8.56[−4]	9.20[−4]	9.71[−4]	1.01[−3]	1.06[−3]	1.11[−3]
	9.03[−4]	8.76[−4]	8.65[−4]	8.56[−4]	8.55[−4]	8.48[−4]	8.24[−4]	7.87[−4]
		6.48[−4][d]						
1–10	4.00[−4]	3.92[−4]	3.85[−4]	3.73[−4]	3.66[−4]	3.60[−4]	3.53[−4]	3.50[−4]
	4.10[−4]	4.04[−4]	3.98[−4]	3.88[−4]	3.81[−4]	3.76[−4]	3.71[−4]	3.67[−4]
	4.85[−4]	4.71[−4]	4.60[−4]	4.27[−4]	4.15[−4]	4.04[−4]	3.87[−4]	3.73[−4]
		3.47[−4][d]						

[a]Notation used in this and subsequent tables, e.g., $1.24[-3]=1.24\times10^{-3}$.

[b]Result by Dirac R-matrix method from Ref. [5].

[c]Results by RDW method from Ref. [10]. The E_i used for each transition were 36.74 Ry, 73.53 Ry, and 367.38 Ry, respectively, which are slightly different from those in this table.

[d]Results by RDW method from Ref. [8].

43% for 1–8, and 44% for 1–10, are found. In contrast, for transitions at low impact energies, most of the discrepancies stay within 10% except for the transitions 1–3, 1–5, and 1–10. This is probably because Bhatia and Mason [16] used insufficient partial waves (only $l\leqslant7$). They used a Coulomb-Bethe procedure to extrapolate their results to higher l resulting in overestimation for transition 1–3 and underestimation for transition 1–5 at low impact energies. In comparison, our result agrees better with the fourth entry for transition 1–3 at $E_i=15$ Ry. Nevertheless, a 20% difference still exists. Although the channel coupling effect was considered by the Dirac R-matrix method [5], the value 8.6×10^{-3} obtained by this method for the transition 1–3 by Norrington and Grant (NG) may have underestimated the collision strength because of insufficient partial-wave expansion (only up to $l=16$). As further verification we recalculated this transition with only partial-wave expansion up to $l=16$ in the present calculation, and obtained a value of 9.8×10^{-3} for the collision strength. If partial-wave expansion up to $l=25$ was used, the collision strength converged to 1.07×10^{-2}. Therefore some of the discrepancy (about 10%) between the present calculation and the NG's calculation is due to the

TABLE II. Comparison of collision strengths for transitions at different E_i between excited levels in the $n=2$ complex. The meaning for each entry is the same as that of Table I.

Transition	E_i (Ry)							
$I-F$	15.0	30.0	45.0	85.0	127.5	170.0	250.0	350.0
2–3	1.27[−2]	1.08[−2]	9.32[−3]	6.57[−3]	4.81[−3]	3.68[−3]	2.41[−3]	1.57[−3]
	1.31[−2]	1.11[−2]	9.55[−3]	6.71[−3]	4.89[−3]	3.73[−3]	2.44[−3]	1.59[−3]
	1.42[−2]	1.20[−2]	1.02[−2]	7.11[−3]	5.11[−3]	3.85[−3]	2.48[−3]	1.60[−3]
2–4	9.53[−3]	9.05[−3]	8.76[−3]	8.21[−3]	7.99[−3]	7.90[−3]	7.87[−3]	7.93[−3]
	9.53[−3]	8.98[−3]	8.63[−3]	8.12[−3]	7.91[−3]	7.83[−3]	7.79[−3]	7.83[−3]
	9.63[−3]	8.96[−3]	8.46[−3]	7.68[−3]	7.14[−3]	6.78[−3]	6.30[−3]	5.87[−3]
2–5	3.13[−3]	2.65[−3]	2.26[−3]	1.56[−3]	1.11[−3]	8.32[−4]	5.25[−4]	3.29[−4]
	3..22[−3]	2.71[−3]	2.30[−3]	1.58[−3]	1.12[−3]	8.33[−4]	5.23[−4]	3.27[−4]
	3.51[−3]	2.94[−3]	2.49[−3]	1.71[−3]	1.19[−3]	8.79[−4]	5.44[−4]	3.37[−4]
2–6	8.44[−4]	7.43[−4]	6.55[−4]	4.78[−4]	3.56[−4]	2.74[−4]	1.81[−4]	1.19[−4]
	8.78[−4]	7.72[−4]	6.78[−4]	4.92[−4]	3.65[−4]	2.81[−4]	1.85[−4]	1.21[−4]
	9.11[−4]	7.94[−4]	6.95[−4]	5.02[−4]	3.69[−4]	2.82[−4]	1.83[−4]	1.19[−4]
2–7	1.49[−1]	1.61[−1]	1.73[−1]	1.99[−1]	2.19[−1]	2.38[−1]	2.57[−1]	2.79[−1]
	1.47[−1]	1.60[−1]	1.74[−1]	2.05[−1]	2.27[−1]	2.49[−1]	2.66[−1]	2.89[−1]
	1.34[−1]	1.48[−1]	1.61[−1]	1.89[−1]	2.09[−1]	2.24[−1]	2.45[−1]	2.64[−1]
2–8	2.32[−3]	2.04[−3]	1.79[−3]	1.31[−3]	9.74[−4]	7.51[−4]	4.96[−4]	3.26[−4]
	2.40[−3]	2.11[−3]	1.85[−3]	1.34[−3]	9.97[−4]	7.67[−4]	5.05[−4]	3.30[−4]
	2.47[−3]	2.16[−3]	1.89[−3]	1.38[−3]	1.02[−3]	7.77[−4]	5.08[−4]	3.29[−4]
2–9	4.99[−4]	4.38[−4]	3.85[−4]	2.80[−4]	2.08[−4]	1.60[−4]	1.06[−4]	6.93[−5]
	5.14[−4]	4.51[−4]	3.95[−4]	2.86[−4]	2.12[−4]	1.63[−4]	1.07[−4]	7.00[−5]
	5.50[−4]	4.79[−4]	4.19[−4]	3.05[−4]	2.24[−4]	1.71[−4]	1.11[−4]	0.72[−4]
2–10	7.88[−5]	6.76[−5]	5.82[−5]	4.06[−5]	2.92[−5]	2.17[−5]	1.38[−5]	8.62[−6]
	8.13[−5]	6.97[−5]	5.99[−5]	4.15[−5]	2.95[−5]	2.20[−5]	1.39[−5]	8.66[−6]
	0.92[−4]	0.77[−4]	0.66[−4]	0.45[−4]	0.31[−4]	0.23[−4]	0.14[−4]	0.09[−4]
3–4	3.64[−2]	3.31[−2]	3.05[−2]	2.61[−2]	2.35[−2]	2.19[−2]	2.03[−2]	1.94[−2]
	3.69[−2]	3.34[−2]	3.06[−2]	2.62[−2]	2.36[−2]	2.19[−2]	2.02[−2]	1.92[−2]
	3.84[−2]	3.42[−2]	3.10[−2]	2.55[−2]	2.18[−2]	1.95[−2]	1.68[−2]	1.48[−2]
3–5	9.78[−3]	8.40[−3]	7.32[−3]	5.35[−3]	4.13[−3]	3.37[−3]	2.55[−3]	2.05[−3]
	1.00[−2]	8.60[−3]	7.46[−3]	5.43[−3]	4.17[−3]	3.40[−3]	2.57[−3]	2.06[−3]
	1.09[−2]	9.22[−3]	7.94[−3]	5.68[−3]	4.23[−3]	3.34[−3]	2.38[−3]	1.74[−3]
3–6	1.55[−1]	1.69[−1]	1.84[−1]	2.11[−1]	2.34[−1]	2.57[−1]	2.74[−1]	3.00[−1]
	1.54[−1]	1.70[−1]	1.89[−1]	2.20[−1]	2.45[−1]	2.71[−1]	2.85[−1]	3.14[−1]
	1.41[−1]	1.55[−1]	1.67[−1]	2.05[−1]	2.26[−1]	2.41[−1]	2.62[−1]	2.82[−1]
3–7	1.12[−1]	1.21[−1]	1.28[−1]	1.48[−1]	1.63[−1]	1.78[−1]	1.91[−1]	2.07[−1]
	1.12[−1]	1.21[−1]	1.30[−1]	1.52[−1]	1.69[−1]	1.88[−1]	1.98[−1]	2.16[−1]
	1.04[−1]	1.14[−1]	1.23[−1]	1.42[−1]	1.56[−1]	1.67[−1]	1.81[−1]	1.95[−1]
3–8	1.93[−1]	2.08[−1]	2.24[−1]	2.57[−1]	2.82[−1]	3.04[−1]	3.29[−1]	3.56[−1]
	1.90[−1]	2.05[−1]	2.25[−1]	2.63[−1]	2.91[−1]	3.16[−1]	3.39[−1]	3.66[−1]
	1.65[−1]	1.82[−1]	1.98[−1]	2.40[−1]	2.65[−1]	2.84[−1]	3.10[−1]	3.33[−1]
3–9	1.18[−2]	1.23[−2]	1.26[−2]	1.35[−2]	1.45[−2]	1.51[−2]	1.65[−2]	1.73[−2]
	1.22[−2]	1.26[−2]	1.30[−2]	1.40[−2]	1.54[−2]	1.60[−2]	1.78[−2]	1.85[−2]
	1.16[−2]	1.17[−2]	1.19[−2]	1.30[−2]	1.36[−2]	1.43[−2]	1.52[−2]	1.62[−2]
3–10	6.79[−4]	6.58[−4]	6.36[−4]	6.03[−4]	5.94[−4]	5.93[−4]	6.01[−4]	6.23[−4]
	7.00[−4]	6.72[−4]	6.45[−4]	6.10[−4]	6.07[−4]	6.10[−4]	6.21[−4]	6.46[−4]
	6.18[−4]	6.02[−4]	5.88[−4]	6.39[−4]	5.00[−4]	4.08[−4]	3.00[−4]	2.23[−4]
4–5	1.65[−2]	1.40[−2]	1.19[−2]	8.32[−3]	6.04[−3]	4.62[−3]	3.07[−3]	2.10[−3]
	1.69[−2]	1.42[−2]	1.21[−2]	8.38[−3]	6.06[−3]	4.60[−3]	3.04[−3]	2.06[−3]
	1.84[−2]	1.54[−2]	1.31[−2]	8.98[−3]	6.36[−3]	4.75[−3]	3.04[−3]	1.98[−3]
4–6	5.21[−4]	4.61[−4]	4.07[−4]	3.00[−4]	2.25[−4]	1.75[−4]	1.17[−4]	7.73[−5]
	5.50[−4]	4.86[−4]	4.29[−4]	3.15[−4]	2.35[−4]	1.82[−4]	1.21[−4]	7.99[−5]
	5.75[−4]	5.03[−4]	4.43[−4]	3.25[−4]	2.41[−4]	1.86[−4]	1.23[−4]	0.80[−4]
4–7	1.92[−1]	2.08[−1]	2.25[−1]	2.64[−1]	2.91[−1]	3.15[−1]	3.38[−1]	3.69[−1]
	1.91[−1]	2.11[−1]	2.31[−1]	2.77[−1]	3.05[−1]	3.33[−1]	3.52[−1]	3.86[−1]
	1.85[−1]	2.05[−1]	2.22[−1]	2.55[−1]	2.79[−1]	2.98[−1]	3.24[−1]	3.47[−1]

TABLE II. (*Continued.*)

Transition	E_i (Ry)							
$I-F$	15.0	30.0	45.0	85.0	127.5	170.0	250.0	350.0
4–8	4.23[−1]	4.63[−1]	4.98[−1]	5.69[−1]	6.31[−1]	6.94[−1]	7.40[−1]	8.06[−1]
	4.21[−1]	4.68[−1]	5.10[−1]	5.90[−1]	6.58[−1]	7.32[−1]	7.68[−1]	8.42[−1]
	4.00[−1]	5.34[−1]	4.80[−1]	5.55[−1]	6.10[−1]	6.52[−1]	7.10[−1]	7.62[−1]
4–9	1.52[−1]	1.62[−1]	1.70[−1]	1.94[−1]	2.13[−1]	2.25[−1]	2.45[−1]	2.63[−1]
	1.50[−1]	1.61[−1]	1.69[−1]	1.97[−1]	2.19[−1]	2.32[−1]	2.53[−1]	2.70[−1]
	1.34[−1]	1.46[−1]	1.56[−1]	1.78[−1]	1.95[−1]	2.08[−1]	2.26[−1]	2.43[−1]
4–10	1.66[−3]	1.45[−3]	1.26[−3]	9.03[−4]	6.61[−4]	5.03[−4]	3.26[−4]	2.10[−4]
	1.71[−3]	1.48[−3]	1.29[−3]	9.19[−4]	6.70[−4]	5.08[−4]	3.28[−4]	2.10[−4]
	1.76[−3]	1.52[−3]	1.32[−3]	9.44[−4]	6.83[−4]	5.15[−4]	3.30[−4]	2.09[−4]
5–6	9.35[−3]	1.07[−2]	1.16[−2]	1.28[−2]	1.42[−2]	1.48[−2]	1.52[−2]	1.57[−2]
	1.21[−2]	1.45[−2]	1.50[−2]	1.53[−2]	1.71[−2]	1.75[−2]	1.73[−2]	1.74[−2]
	1.10[−2]	1.18[−2]	1.25[−2]	1.54[−2]	1.33[−2]	1.18[−2]	9.70[−3]	7.93[−3]
		1.17[−2][a]						
5–7	6.16[−3]	6.35[−3]	6.52[−3]	6.56[−3]	6.51[−3]	6.66[−3]	6.72[−3]	6.72[−3]
	6.53[−3]	6.98[−3]	7.11[−3]	6.96[−3]	6.81[−3]	7.02[−3]	6.96[−3]	6.82[−3]
	6.97[−3]	6.87[−3]	6.78[−3]	8.58[−3]	6.79[−3]	5.58[−3]	4.13[−3]	3.08[−3]
		6.40[−3][a]						
5–8	1.60[−1]	1.85[−1]	2.01[−1]	2.43[−1]	2.55[−1]	2.75[−1]	2.99[−1]	3.12[−1]
	1.76[−1]	2.05[−1]	2.26[−1]	2.69[−1]	2.72[−1]	2.95[−1]	3.19[−1]	3.26[−1]
	1.59[−1]	1.77[−1]	1.91[−1]	2.18[−1]	2.38[−1]	2.52[−1]	2.72[−1]	2.89[−1]
		2.04[−1][a]						
5–9	6.22[−1]	6.94[−1]	7.54[−1]	8.91[−1]	1.01+0	1.05+0	1.16+0	1.24+0
	6.39[−1]	7.22[−1]	7.95[−1]	9.47[−1]	1.08+0	1.10+0	1.22+0	1.31+0
	5.97[−1]	6.71[−1]	7.32[−1]	8.52[−1]	9.37[−1]	9.99[−1]	1.09+0	1.16+0
5–10	2.46[−1]	2.69[−1]	2.87[−1]	3.32[−1]	3.65[−1]	3.99[−1]	4.30[−1]	4.67[−1]
	2.52[−1]	2.78[−1]	2.99[−1]	3.53[−1]	3.92[−1]	4.33[−1]	4.61[−1]	5.02[−1]
	2.36[−1]	2.59[−1]	2.78[−1]	2.85[−1]	3.52[−1]	3.76[−1]	4.10[−1]	4.41[−1]
6–7	1.35[−2]	1.16[−2]	1.00[−2]	7.11[−3]	5.22[−3]	4.01[−3]	2.63[−3]	1.72[−3]
	1.39[−2]	1.19[−2]	1.02[−2]	7.24[−3]	5.30[−3]	4.05[−3]	2.65[−3]	1.73[−3]
	1.59[−2]	1.34[−2]	1.15[−2]	7.93[−3]	5.71[−3]	4.31[−3]	2.78[−3]	1.79[−3]
6–8	1.39[−2]	1.29[−2]	1.22[−2]	1.09[−2]	1.02[−2]	9.86[−3]	9.51[−3]	9.36[−3]
	1.42[−2]	1.31[−2]	1.24[−2]	1.11[−2]	1.04[−2]	1.00[−2]	9.66[−3]	9.49[−3]
	1.50[−2]	1.36[−2]	1.25[−2]	1.07[−2]	9.48[−3]	8.73[−3]	7.81[−3]	7.09[−3]
6–9	2.72[−3]	2.28[−3]	1.94[−3]	1.32[−3]	9.42[−4]	7.06[−4]	4.53[−4]	2.97[−4]
	2.83[−3]	2.37[−3]	2.01[−3]	1.36[−3]	9.66[−4]	7.22[−4]	4.62[−4]	3.03[−4]
	3.32[−3]	2.75[−3]	2.31[−3]	1.51[−3]	1.05[−3]	7.68[−4]	4.74[−4]	2.96[−4]
6–10	5.06[−4]	4.16[−4]	3.47[−4]	2.25[−4]	1.52[−4]	1.09[−4]	6.33[−5]	4.02[−5]
	5.31[−4]	4.36[−4]	3.62[−4]	2.35[−4]	1.59[−4]	1.18[−4]	6.79[−5]	5.24[−5]
	6.32[−4]	5.11[−4]	4.19[−4]	2.62[−4]	1.72[−4]	1.20[−4]	6.80[−5]	3.90[−5]
7–8	3.90[−2]	3.48[−2]	3.16[−2]	2.58[−2]	2.21[−2]	1.98[−2]	1.74[−2]	1.59[−2]
	4.02[−2]	3.57[−2]	3.23[−2]	2.78[−2]	2.29[−2]	2.04[−2]	1.78[−2]	1.62[−2]
	4.37[−2]	3.81[−2]	3.39[−2]	2.63[−2]	2.15[−2]	1.85[−2]	1.50[−2]	1.27[−2]
7–9	2.21[−2]	1.92[−2]	1.70[−2]	1.29[−2]	1.04[−2]	8.86[−3]	7.20[−3]	6.19[−3]
	2.29[−2]	1.97[−2]	1.74[−2]	1.32[−2]	1.05[−2]	8.94[−3]	7.26[−3]	6.23[−3]
	2.53[−2]	2.16[−2]	1.87[−2]	1.37[−2]	1.05[−2]	8.60[−3]	6.47[−3]	5.08[−3]
7–10	3.20[−3]	2.66[−3]	2.23[−3]	1.49[−3]	1.03[−3]	7.46[−4]	4.51[−4]	2.71[−4]
	3.32[−3]	2.75[−3]	2.30[−3]	1.52[−3]	1.05[−3]	7.57[−4]	4.55[−4]	2.72[−4]
	3.81[−3]	3.12[−3]	1.13[−3]	1.67[−3]	1.13[−3]	8.05[−4]	4.74[−4]	2.79[−4]
8–9	5.25[−2]	4.74[−2]	4.35[−2]	3.65[−2]	3.26[−2]	3.03[−2]	2.78[−2]	2.63[−2]
	5.30[−2]	4.77[−2]	4.38[−2]	3.68[−2]	3.27[−2]	3.03[−2]	2.78[−2]	2.62[−2]
	5.85[−2]	5.14[−2]	4.61[−2]	3.67[−2]	3.09[−2]	2.73[−2]	2.31[−2]	2.01[−2]
8–10	7.07[−3]	6.43[−3]	5.96[−3]	5.17[−3]	4.73[−3]	4.51[−3]	4.33[−3]	4.28[−3]
	7.18[−3]	6.55[−3]	6.22[−3]	5.22[−3]	4.74[−3]	4.50[−3]	4.31[−3]	4.26[−3]
	8.02[−3]	7.05[−3]	6.33[−3]	5.09[−3]	4.40[−3]	3.99[−3]	3.53[−3]	3.20[−3]
9–10	1.93[−2]	1.94[−2]	1.96[−2]	2.01[−2]	2.07[−2]	2.13[−2]	2.22[−2]	2.31[−2]
	1.95[−2]	1.94[−2]	1.95[−2]	2.03[−2]	2.08[−2]	2.14[−2]	2.24[−2]	2.33[−2]
	1.91[−2]	1.86[−2]	1.84[−2]	1.84[−2]	1.82[−2]	1.81[−2]	1.77[−2]	1.70[−2]

[a]Results by RDW method from Ref. [8].

TABLE III. Comparison of collision strengths for transitions at different E_i from levels in $2s^2$ or $2s2p$ to levels in $2s3l$ ($l=s,p,d$), which include resonance transitions and transitions between excited levels. The meaning for each entry is the same as that of Table I.

Transition	E_i (Ry)					Transition	E_i (Ry)				
$I-F$	85.0	127.5	170.0	250.0	350.0	$I-F$	85.0	127.5	170.0	250.0	350.0
1–11	1.15[−3]	6.93[−4]	4.67[−4]	2.66[−4]	1.57[−4]		2.04[−3]	1.16[−3]	7.40[−4]	3.81[−4]	2.04[−4]
	1.12[−3]	6.68[−4]	4.47[−4]	2.53[−4]	1.49[−4]		2.16[−3]	1.23[−3]	7.77[−4]	3.93[−4]	2.04[−4]
	1.08[−3]	6.58[−4]	4.41[−4]	2..45[−4]	1.40[−4]	2–19	1.92[−3]	1.55[−3]	1.43[−3]	1.39[−3]	1.42[−3]
1–12	1.35[−2]	1.48[−2]	1.56[−2]	1.64[−2]	1.70[−2]		1.93[−3]	1.54[−3]	1.41[−3]	1.37[−3]	1.39[−3]
	1.28[−2]	1.40[−2]	1.48[−2]	1.57[−2]	1.62[−2]		1.89[−3]	1.36[−3]	1.12[−3]	9.35[−4]	8.16[−4]
	1.10[−2]	1.27[−2]	1.37[−2]	1.45[−2]	1.50[−2]	2–20	1.94[−3]	1.10[−3]	7.00[−4]	3.59[−4]	1.90[−4]
1–13	3.50[−3]	5.36[−3]	7.14[−3]	1.01[−2]	1.31[−2]		1.94[−3]	1.10[−3]	6.97[−4]	3.56[−4]	1.89[−4]
	1.70[−3]	2.10[−3]	2.56[−3]	3.43[−3]	4.37[−3]		2.05[−3]	1.17[−3]	7.36[−4]	3.70[−4]	1.91[−4]
	4.26[−3]	4.69[−3]	5.52[−3]	7.13[−3]	9.49[−3]	3–11	1.41[−3]	1.74[−3]	2.17[−3]	3.02[−3]	3.93[−3]
1–14	2.86[−4]	1.80[−4]	1.22[−4]	6.79[−5]	3.84[−5]		1.21[−3]	1.37[−3]	1.63[−3]	2.19[−3]	2.80[−3]
	2.81[−4]	1.77[−4]	1.20[−4]	6.68[−5]	3.78[−5]		1.48[−3]	1.52[−3]	1.69[−3]	2.22[−3]	3.06[−3]
	2.87[−4]	1.75[−4]	1.17[−4]	6.32[−5]	3.37[−5]	3–12	3.77[−4]	2.61[−4]	1.92[−4]	1.26[−4]	8.94[−5]
1–15	4.58[−3]	7.57[−3]	1.04[−2]	1.50[−2]	1.96[−2]		3.50[−4]	2.46[−4]	1.87[−4]	1.32[−4]	1.05[−4]
	6.08[−3]	1.04[−2]	1.45[−2]	2.12[−2]	2.81[−2]		3.68[−4]	2.49[−4]	1.82[−4]	1.16[−4]	7.63[−5]
	4.65[−3]	7.34[−3]	9.79[−3]	1.39[−2]	1.93[−2]	3–13	1.78[−2]	1.83[−2]	1.86[−2]	1.91[−2]	1.94[−2]
1–16	1.41[−3]	8.81[−4]	5.98[−4]	3.32[−4]	1.87[−4]		2.20[−2]	2.29[−2]	2.34[−2]	2.41[−2]	2.47[−2]
	1.37[−3]	8.63[−4]	5.87[−4]	3.26[−4]	1.84[−4]		1.54[−2]	1.65[−2]	1.71[−2]	1.76[−2]	1.78[−2]
	1.45[−3]	8.90[−4]	5.99[−4]	3.23[−4]	1.71[−4]	3–14	8.36[−4]	5.20[−4]	3.54[−4]	1.99[−4]	1.15[−4]
1–17	1.64[−3]	9.80[−4]	6.52[−4]	3.57[−4]	2.02[−4]		8.09[−4]	5.02[−4]	3.40[−4]	1.90[−4]	1.10[−4]
	1.64[−3]	1.01[−3]	6.67[−4]	3.65[−4]	2.06[−4]		8.46[−4]	5.25[−4]	3.53[−4]	1.93[−4]	1.08[−4]
	1.66[−3]	1.00[−3]	6.59[−4]	3.49[−4]	1.87[−4]	3–15	1.06[−2]	1.05[−2]	1.04[−2]	1.05[−2]	1.06[−2]
1–18	2.75[−3]	1.74[−3]	1.21[−3]	7.53[−4]	5.16[−4]		3.25[−3]	2.49[−3]	2.11[−3]	1.79[−3]	1.63[−3]
	2.84[−3]	1.79[−3]	1.25[−3]	7.83[−4]	5.46[−4]		1.07[−2]	8.04[−3]	6.47[−3]	4.97[−3]	4.14[−3]
	2.79[−3]	1.73[−3]	1.16[−3]	6.52[−4]	3.78[−4]	3–16	4.75[−3]	4.12[−3]	3.92[−3]	3.91[−3]	4.05[−3]
1–19	3.84[−3]	2.30[−3]	1.53[−3]	8.37[−4]	4.74[−4]		4.24[−3]	3.46[−3]	3.16[−3]	3.01[−3]	3.04[−3]
	3.95[−3]	2.33[−3]	1.54[−3]	8.41[−4]	4.75[−4]		5.02[−3]	3.58[−3]	2.60[−3]	1.55[−3]	9.76[−4]
	3.85[−3]	2.31[−3]	1.52[−3]	8.08[−4]	4.32[−4]	3–17	2.07[−2]	2.51[−2]	2.93[−2]	3.63[−2]	4.34[−2]
1–20	1.69[−3]	2.27[−2]	2.70[−2]	3.25[−2]	3.69[−2]		1.94[−2]	2.33[−2]	2.70[−2]	3.32[−2]	3.94[−2]
	1.68[−2]	2.27[−2]	2.70[−2]	3.26[−2]	3.71[−2]		2.01[−2]	2.38[−2]	2.69[−2]	3.19[−2]	3.78[−2]
	1.66[−2]	1.91[−2]	1.87[−2]	1.68[−2]	1.49[−2]	3–18	5.69[−2]	7.32[−2]	8.73[−2]	1.10[−1]	1.31[−1]
2–11	4.71[−4]	5.79[−4]	7.23[−4]	1.00[−3]	1.31[−3]		5.36[−2]	6.85[−2]	8.11[−2]	1.01[−1]	1.21[−1]
	4.05[−4]	4.55[−4]	5.41[−4]	7.29[−4]	9.30[−4]		5.45[−2]	6.88[−2]	7.96[−2]	9.62[−2]	1.15[−1]
	4.90[−4]	5.00[−4]	5.57[−4]	7.20[−4]	9.76[−4]	3–19	7.24[−3]	5.05[−3]	4.09[−3]	3.40[−3]	3.14[−3]
2–12	1.23[−4]	8.33[−5]	5.91[−5]	3.47[−5]	2.06[−5]		7.23[−3]	5.01[−3]	4.05[−3]	3.35[−3]	3.10[−3]
	1.14[−4]	7.67[−5]	5.44[−5]	3.19[−5]	1.89[−5]		7.33[−3]	4.74[−3]	3.53[−3]	2.53[−3]	1.98[−3]
	1.24[−4]	0.82[−4]	0.57[−4]	0.33[−4]	0.19[−4]	3–20	6.07[−3]	3.82[−3]	2.78[−3]	1.97[−3]	1.64[−3]
2–13	6.86[−4]	4.18[−4]	2.79[−4]	1.53[−4]	8.65[−5]		6.20[−3]	3.99[−3]	2.99[−3]	2.27[−3]	2.03[−3]
	7.77[−4]	4.78[−4]	3.23[−4]	1.79[−4]	1.02[−4]		6.30[−3]	4.04[−3]	2.98[−3]	1.92[−3]	1.83[−3]
	6.82[−4]	4.21[−4]	2.81[−4]	1.53[−4]	0.85[−4]	4–11	2.41[−3]	3.05[−3]	3.84[−3]	5.33[−3]	6.98[−3]
2–14	8.12[−3]	8.63[−3]	8.94[−3]	9.27[−3]	9.49[−3]		2.08[−3]	2.42[−3]	2.93[−3]	3.97[−3]	5.11[−3]
	7.08[−3]	7.52[−3]	7.78[−3]	8.07[−3]	8.27[−3]		2.57[−3]	2.69[−3]	3.06[−3]	4.22[−3]	6.05[−3]
	6.44[−3]	7.16[−3]	7.54[−3]	7.91[−3]	8.10[−3]	4–12	6.08[−4]	4.08[−4]	2.88[−4]	1.69[−4]	9.97[−5]
2–15	1.06[−3]	6.63[−4]	4.55[−4]	2.60[−4]	1.53[−4]		5.76[−4]	3.86[−4]	2.72[−4]	1.59[−4]	9.37[−5]
	8.51[−4]	5.30[−4]	3.60[−4]	2.02[−4]	1.17[−4]		6.18[−4]	4.05[−4]	2.83[−4]	1.61[−4]	9.16[−5]
	1.01[−3]	6.42[−4]	4.36[−4]	2.42[−4]	1.37[−4]	4–13	4.84[−3]	3.80[−3]	3.33[−3]	3.00[−3]	2.91[−3]
2–16	1.61[−3]	1.53[−3]	1.55[−3]	1.64[−3]	1.76[−3]		4.38[−3]	3.54[−3]	3.19[−3]	3.00[−3]	2.99[−3]
	1.38[−3]	1.23[−3]	1.19[−3]	1.22[−3]	1.29[−3]		4.75[−3]	3.43[−3]	2.52[−3]	1.54[−3]	9.92[−4]
	1.69[−3]	1.26[−3]	9.27[−4]	5.59[−4]	3.58[−4]	4–14	1.65[−3]	1.57[−3]	1.59[−3]	1.69[−3]	1.81[−3]
2–17	2.44[−2]	3.20[−2]	3.84[−2]	4.86[−2]	5.85[−2]		1.45[−3]	1.31[−3]	1.29[−3]	1.34[−3]	1.41[−3]
	2.26[−2]	2.95[−2]	3.52[−2]	4.43[−2]	5.31[−2]		1.67[−3]	1.28[−3]	9.63[−4]	6.09[−4]	4.11[−4]
	2.33[−2]	3.00[−2]	3.50[−2]	4.24[−2]	5.06[−2]	4–15	3.80[−3]	2.77[−3]	2.29[−3]	1.93[−3]	1.79[−3]
2–18	2.06[−3]	1.18[−3]	7.50[−4]	3.86[−4]	2.07[−4]		3.75[−3]	2.39[−3]	1.71[−3]	1.10[−3]	7.92[−4]

TABLE III. (*Continued.*)

Transition	E_i (Ry)					Transition	E_i (Ry)				
$I-F$	85.0	127.5	170.0	250.0	350.0	$I-F$	85.0	127.5	170.0	250.0	350.0
	4.07[−3]	2.60[−3]	1.76[−3]	9.77[−4]	5.54[−4]		3.27[−3]	2.64[−3]	2.34[−3]	2.10[−3]	2.00[−3]
4–16	4.62[−2]	4.73[−2]	4.82[−2]	4.94[−2]	5.04[−2]		3.34[−3]	2.45[−3]	1.94[−3]	1.43[−3]	1.16[−3]
	4.13[−2]	4.21[−2]	4.28[−2]	4.37[−2]	4.45[−2]	5–14	7.41[−4]	4.65[−4]	3.18[−4]	1.80[−4]	1.04[−4]
	4.32[−2]	4.49[−2]	4.55[−2]	4.59[−2]	4.61[−2]		7.74[−4]	4.82[−4]	3.27[−4]	1.84[−4]	1.06[−4]
4–17	5.71[−3]	5.02[−3]	4.93[−3]	5.19[−3]	5.65[−3]		7.80[−4]	4.82[−4]	3.23[−4]	1.77[−4]	0.98[−4]
	5.70[−3]	4.94[−3]	4.80[−3]	5.01[−3]	5.42[−3]	5–15	1.02[−2]	1.04[−2]	1.05[−2]	1.08[−2]	1.10[−2]
	5.60[−3]	4.55[−3]	4.17[−3]	4.04[−3]	4.16[−3]		2.34[−2]	2.47[−2]	2.57[−2]	2.68[−2]	2.76[−2]
4–18	2.65[−2]	2.98[−2]	3.36[−2]	4.03[−2]	4.74[−2]		7.76[−3]	8.35[−3]	8.58[−3]	8.73[−3]	8.79[−3]
	2.55[−2]	2.83[−2]	3.17[−2]	3.78[−2]	4.41[−2]	5–16	3.55[−3]	2.24[−3]	1.55[−3]	9.10[−4]	5.66[−4]
	2.57[−2]	2.80[−2]	3.04[−2]	3.51[−2]	4.11[−2]		3.68[−3]	2.29[−3]	1.57[−3]	9.10[−4]	5.58[−4]
4–19	1.13[−1]	1.42[−1]	1.67[−1]	2.08[−1]	2.48[−1]		3.87[−3]	2.39[−3]	1.59[−3]	8.66[−4]	4.82[−4]
	1.07[−1]	1.34[−1]	1.57[−1]	1.95[−1]	2.32[−1]	5–17	3.88[−3]	2.56[−3]	1.96[−3]	1.52[−3]	1.38[−3]
	1.06[−1]	1.34[−1]	1.41[−1]	1.86[−1]	2.22[−1]		4.09[−3]	2.68[−3]	2.05[−3]	1.59[−3]	1.44[−3]
4–20	9.16[−3]	5.26[−3]	3.39[−3]	1.82[−3]	1.07[−3]		4.28[−3]	2.70[−3]	1.98[−3]	1.45[−3]	1.29[−3]
	9.29[−3]	5.32[−3]	3.44[−3]	1.86[−3]	1.12[−3]	5–18	5.83[−3]	3.69[−3]	2.70[−3]	1.94[−3]	1.64[−3]
	9.56[−3]	5.52[−3]	3.52[−3]	1.86[−3]	1.07[−3]		5.95[−3]	3.64[−3]	2.56[−3]	1.69[−3]	1.32[−3]
5–11	9.68[−4]	6.70[−4]	5.01[−4]	3.40[−4]	2.57[−4]		6.63[−3]	3.93[−3]	3.09[−3]	1.68[−3]	1.28[−3]
	1.00[−3]	6.89[−4]	5.11[−4]	3.40[−4]	2.52[−4]	5–19	7.07[−3]	4.07[−3]	2.62[−3]	1.39[−3]	7.81[−4]
	1.01[−3]	6.77[−4]	4.84[−4]	3.19[−4]	2.37[−4]		7.34[−3]	4.19[−3]	2.67[−3]	1.40[−3]	7.81[−4]
5–12	5.39[−4]	7.69[−4]	1.01[−3]	1.44[−3]	1.90[−3]		7.87[−3]	4.38[−3]	2.74[−3]	1.37[−3]	7.24[−4]
	6.47[−4]	9.87[−4]	1.33[−3]	1.94[−3]	2.58[−3]	5–20	6.98[−2]	8.93[−2]	1.06[−1]	1.31[−1]	1.55[−1]
	4.26[−4]	6.14[−4]	8.36[−4]	1.31[−3]	1.98[−3]		7.92[−2]	1.03[−1]	1.22[−1]	1.52[−1]	1.81[−1]
5–13	4.18[−3]	3.87[−3]	3.77[−3]	3.74[−3]	3.79[−3]		6.04[−2]	7.96[−2]	9.32[−2]	1.13[−1]	1.35[−1]

channel coupling neglected in our calculation while the remainder (the other 10%) may be attributed to the insufficient partial-wave used in NG's calculation. This phenomenon was also noted by Bhatia and Mason [15] when comparing their result for this transition with that obtained by the Breit-Pauli R-matrix method [7]. There are large differences for the transitions 1–9 and 1–10 between the present RDW result and Zhang and Sampson's result obtained by the same method. The reason for these differences is mainly because only ten-level MCDF configuration expansion was used in Zhang and Sampson's calculation, and so not enough correlation effect was caught.

In Table II, the collision strengths at eight electron-impact energies E_i between excited levels in the $n=2$ complex are presented. The meaning for each entry in each transition is the same as that in Table I. Also, for transitions from level 5 to levels 6–8, selected collision strengths calculated by another RDW method [8] are given in the fourth entries for comparisons. Like the comparisons made in Table I, the results in the first and the second entries are generally in good agreement to within 5% except that for some transitions at high impact energies a 10% difference may be found. The good agreement is partly due to the properly calculated orbitals related to these transitions resulting in good agreement of the oscillator strengths (gf). This can be seen in Table VI of Ref. [3], where the electric dipoles gf in the $n=2$ complex were calculated in the 133-level MCDF CE and 20-level MCDF CE, respectively. When comparisons between the first or second entries and the third entries for each transition are made at high impact energies, the discrepancies are far larger than those in Table I. Indeed, they are greater than 10% for about half of the total transitions. Some discrepancies are even a few times, such as for transitions 3–10 (2.8 times), 5–6 (2 times), and 5–7 (2.2 times). In comparison, at low impact energies, the discrepancies are relatively small though again they are greater than 10% for nearly half of the total transitions. Again, this is probably because Bhatia and Mason [16] used insufficient partial waves (only $l\leqslant 7$). In addition, the lack of full relativistic effect in Ref. [16] may be responsible for part of these discrepancies. In the comparison with the result of the fourth entries calculated by Zhang and Sampson [8] for transitions from level 5 to levels 6–8 at electron impact energy 30 Ry, quite different cases appear. Our results approach those in Ref. [8] for transitions 5–7 and 5–8 but BM's result approaches that in Ref. [8] for transition 5–6. So, from the comparisons of gf in Table VI of Ref. [3], we find that different results may appear no matter whether the gf values are the same or not in the different EIE calculation models, since the collision strengths and gf are the integrated results, and are sensitive to different parts of the orbital wave functions.

Some different conclusions may be drawn from an inspection of Table III, which gives the collision strengths for resonance transitions and transitions between excited levels from levels in $2s^2$ or $2s2p$ to levels in $2s3l$ ($l=s,p,d$) at five different electron-impact energies. In contrast to the comparisons made in the previous two tables, the results in the second entries are quite different from those in the first entries, especially for transitions at low impact energies. Differences of more than a few times are found for some transitions. Most of these transitions have final transition levels 13–16. It is interesting to note that there are very strong configuration interaction (CI) and relativistic and higher-

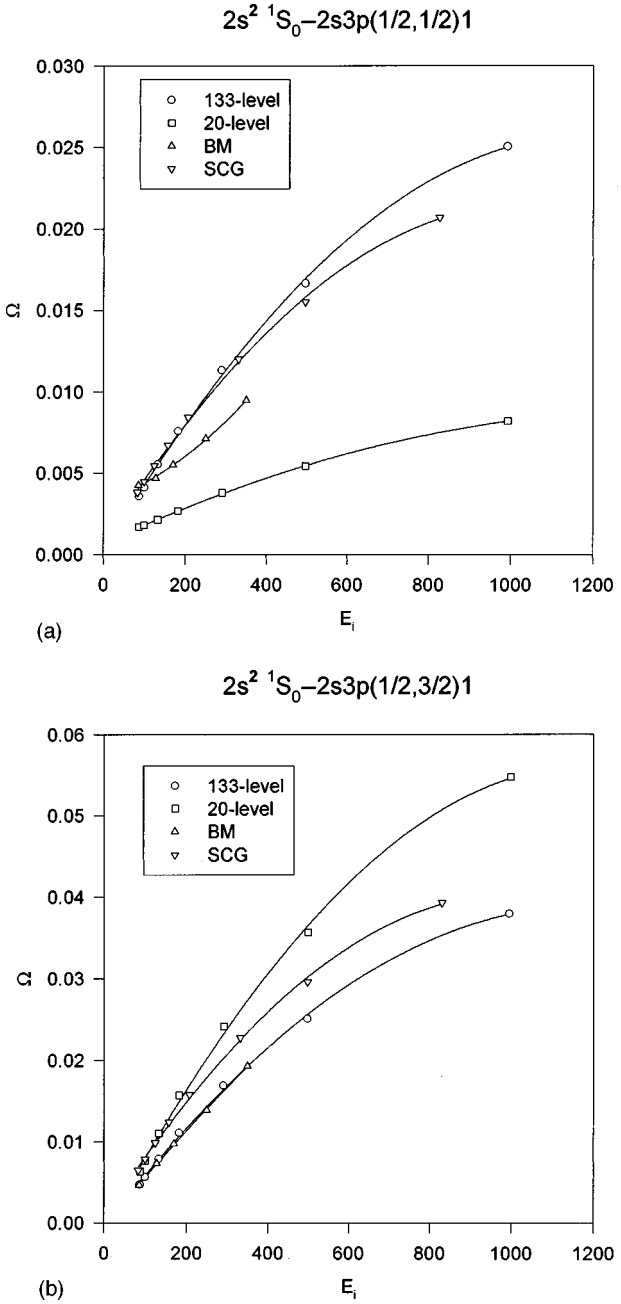

FIG. 1. Plots of collision strengths Ω (dimensionless) against incident electron energy E_i in Ry for two resonance transitions from ground state to states $2s3p(1/2,1/2)1$ (a) and $2s3p(1/2,3/2)1$ (b), respectively. Curves labeled ''133-level'' and ''20-level'' are calculated by the 133-level and 20-level MCDF configuration expansion, respectively, in the present RDW calculations; curve labeled ''BM'' refers to the 46-level nonrelativistic DW calculations by Bhatia and Mason [16] and curve labeled ''SCG'' refers to the nonrelativistic Coulomb-Born-exchange calculations by Sampson *et al.* [11].

order relativistic effects in levels 13-16, which have been extensively analyzed from their energy levels and the dipole transitions related to these levels in Ref. [3]. This evidence indicates that the orbitals related to these transitions as calculated by the 133-level MCDF CE and the 20-level MCDF CE procedures are quite different. Therefore, the 133-level MCDF CE procedure is necessary for EIE calculation for the transitions in Table III. When the comparisons are made between the results in 133-level MCDF CE and those in the third entries of each transition calculated by Bhatia and Mason [16], significant differences larger than those in the previous two tables can be found, especially at high electron impact energies. Comparisons of the corresponding gf in Table V of Ref. [3] also show large differences. Hence, the orbital wave functions for the resonance transitions to high levels or transitions between excited levels are obviously more sensitive to the calculated models than those between relatively low levels. Also, the present calculation by RDW instead of nonrelativistic DW may be responsible for part of these great differences, because the continuum electron orbitals are solved from coupled Dirac equations [17]. In Fig. 1(a) and Fig. 1(b), we show the collision strengths versus the incident electron energy for transitions from the ground state to jj-coupling states $2s2p(1/2,1/2)1$ [3] and $2s3p(1/2,3/2)1$, respectively, by four calculation models, i.e., the 133-level MCDF CE and 20-level MCDF CE models in the present RDW calculations, 46-level nonrelativistic DW calculations by Bhatia and Mason [16], and nonrelativistic Coulomb-Born-exchange calculations by Sampson *et al.* [11]. It is interesting to note that the trends of the results of Sampson *et al.* [11] are closer to those of the present 133-level MCDF CE model than the 20-level MCDF CE model, and even closer than those of Bhatia and Mason's calculation [16] for the transition from $2s^2\ ^1S_0$ to $2s3p(1/2,1/2)1$. From the above comparisons, we come to the conclusion that the RDW method with the atomic structure calculated in 133-level MCDF CE is necessary to calculate accurate collision strengths for the transitions in Table III.

The Coulomb-Born-exchange collision strengths for Fe XXIII calculated by Sampson *et al.* [11] are based on an assumption that the zero-order continuum wave functions are antisymmetric sums of an $N+1$ hydrogenic-ion wave function, of which one is a free Coulomb function and the other N are hydrogenic bound-state functions. Spin-orbit interaction is introduced as a perturbation. As mentioned above, their results are close to ours with 133-level MCDF CE for resonance transitions to levels 13 and 15. We next compare their other results, if calculated, with ours using the 133-level MCDF CE procedure. As shown in Fig. 2(a), their results for the transition $2p^2(1/2,1/2)0-2p3d(1/2,1/2)1$ are again in close agreement with ours because the correlation and relativistic effects are not yet important for this transition. In Figs. 2(b) and 2(d), we compare the collision strengths for the transitions from levels $2p^2(1/2,1/2)0$ and $2p^2(3/2,3/2)0$, respectively, to level $2p3d(3/2,3/2)1$. In both cases, the curves for the collision strengths as a function of impact electron energies E_i decrease at first and then increase with increasing E_i. Although the trends of collision strengths plotted against E_i are the same, there are great differences in magnitude between the two methods used, especially at high E_i, because the overall collision strengths for the two transitions are small and the other configurations included in the MCDF CE in Eq. (2.3) of Ref. [3] contribute more significantly. The contributions calculated with the two methods at high E_i are quite different. Their collision strengths for transition $2p^2(1/2,1/2)0-2p3d(3/2,5/2)1$, as shown in Fig.2(c), are similar to ours, but their E_i dependence is qualitatively different from that observed in our result.

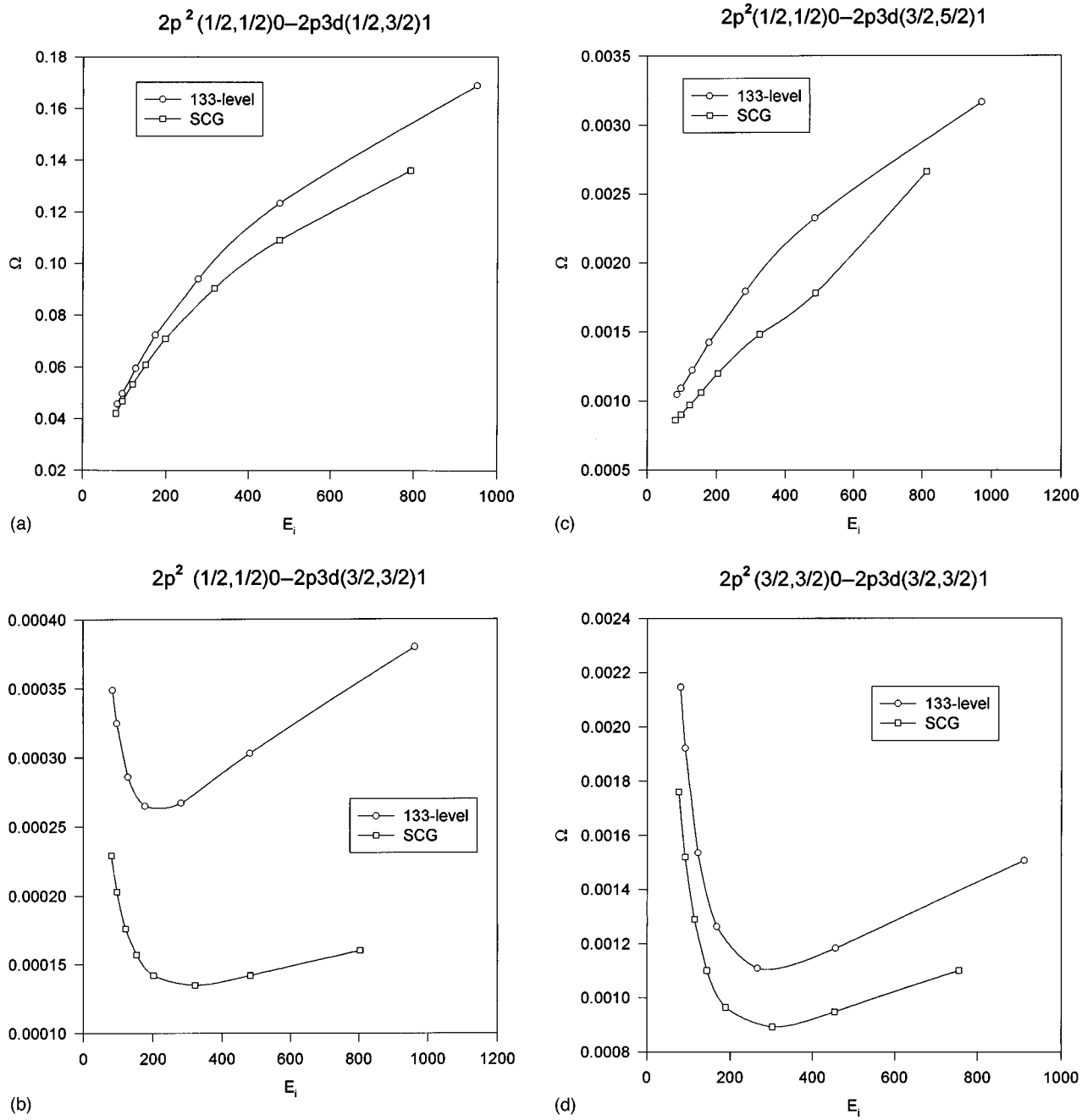

FIG. 2. Plots of collision strengths Ω (dimensionless) against incident electron energy E_i in Ry for four transitions between excited levels from state $2p^2(1/2,1/2)0$ to states $2p3d(1/2,3/2)1$, $2p3d(3/2,3/2)1$, and $2p3d(3/2,5/2)1$ (a)–(c) and from state $2p^2(3/2,3/2)0$ to state $2p3d(3/2,3/2)1$ (d), respectively. Curve labeled ''133-level'' is calculated by the 133-level MCDF configuration-expansion in the present RDW calculations and curve labeled ''SCG'' is from the nonrelativistic Coulomb-Born-exchange calculations by Sampson *et al.* [11].

In Table IV, we present the collision strengths at five electron impact energies E_i for transitions from excited levels in $2p^2$ or $2s3l$ $(l=s,p,d)$ to excited levels in $2s3l$ $(l=s,p,d)$. No other results are available in the literature for comparisons. The results by 20-level MCDF CE in the second entries of each transition are greatly different from those in the first entries, which were calculated by 133-level MCDF CE. The differences are larger than those in the previous tables. Even the qualitative trends of the collision strengths against the impact electron energies E_i for some large-collision-strength transitions are different. For example, for transition 13–18, in which the collision strengths in both of the two calculation modes are very large, the collision strengths increase with increasing E_i in the first entries and decrease in the second entries. This represents strong evidence that it is necessary to use the 133-level MCDF CE mode to obtain the collision strengths between high excited levels in RDW calculations.

IV. SUMMARY

The relativistic distorted-wave method has been used for the calculation of excitation processes for Fe XXIII in the dy-

TABLE IV. Comparison of collision strengths for transitions at five different E_i from excited levels in $2p^2$ or $2s3l$ ($l=s,p,d$) to excited levels in $2s3l(l=s,p,d)$. The meanings for the first and second entries are the same as those of Table I.

Transition	E_i (Ry)					Transition	E_i (Ry)				
$I-F$	85.0	127.5	170.0	250.0	350.0	$I-F$	85.0	127.5	170.0	250.0	350.0
6–11	7.66[−6]	4.59[−6]	3.01[−6]	1.61[−6]	8.95[−7]	8–17	6.72[−5]	4.73[−5]	3.73[−5]	2.88[−5]	2.47[−5]
	6.18[−6]	3.79[−6]	2.59[−6]	1.50[−6]	8.98[−7]		4.90[−7]	2.79[−7]	1.80[−7]	9.63[−8]	5.43[−8]
6–12	8.11[−6]	7.68[−6]	7.52[−6]	7.49[−6]	7.55[−6]	8–18	7.19[−5]	5.51[−5]	4.72[−5]	4.12[−5]	3.92[−5]
	1.04[−4]	1.11[−4]	1.16[−4]	1.21[−4]	1.24[−4]		1.15[−6]	7.83[−7]	6.09[−7]	4.61[−7]	3.88[−7]
6–13	6.56[−5]	7.03[−5]	7.52[−5]	8.39[−5]	9.32[−5]	8–19	5.19[−5]	4.08[−5]	3.60[−5]	3.28[−5]	3.22[−5]
	1.99[−5]	2.56[−5]	3.12[−5]	4.04[−5]	4.98[−5]		1.13[−6]	6.44[−7]	4.16[−7]	2.22[−7]	1.25[−7]
6–14	2.95[−6]	1.74[−6]	1.17[−6]	6.24[−7]	3.43[−7]	8–20	7.92[−4]	7.97[−4]	8.03[−4]	8.10[−4]	8.17[−4]
	1.61[−6]	1.02[−6]	6.92[−7]	3.87[−7]	2.21[−7]		4.95[−5]	4.99[−5]	5.02[−5]	5.08[−5]	5.15[−5]
6–15	7.44[−5]	7.62[−5]	7.98[−5]	8.74[−5]	9.68[−5]	9–11	4.20[−5]	2.57[−5]	1.73[−5]	9.71[−6]	5.66[−6]
	5.98[−5]	9.46[−5]	1.26[−4]	1.76[−4]	2.26[−4]		7.55[−7]	4.00[−7]	2.48[−7]	1.27[−7]	6.89[−8]
6–16	1.67[−5]	1.05[−5]	7.22[−6]	4.10[−6]	2.40[−6]	9–12	7.76[−5]	9.28[−5]	1.04[−4]	1.20[−4]	1.32[−4]
	8.03[−6]	5.00[−6]	3.38[−6]	1.86[−6]	1.05[−6]		1.52[−5]	1.90[−5]	2.19[−5]	2.58[−5]	2.90[−5]
6–17	3.20[−5]	2.06[−5]	1.43[−5]	8.21[−6]	4.79[−6]	9–13	1.04[−4]	1.45[−4]	1.87[−4]	2.59[−4]	3.33[−4]
	9.06[−6]	5.52[−6]	3.70[−6]	2.04[−6]	1.16[−6]		6.48[−6]	8.43[−6]	1.05[−5]	1.39[−5]	1.74[−5]
6–18	3.90[−5]	3.48[−5]	3.34[−5]	3.34[−5]	3.46[−5]	9–14	1.08[−5]	5.98[−6]	3.70[−6]	1.82[−6]	9.33[−7]
	1.54[−5]	9.80[−6]	7.05[−6]	4.55[−6]	3.30[−6]		4.23[−7]	2.16[−7]	1.29[−7]	6.23[−8]	3.22[−8]
6–19	2.12[−5]	1.26[−5]	8.29[−6]	4.46[−6]	2.51[−6]	9–15	2.61[−4]	4.26[−4]	5.78[−4]	8.23[−4]	1.07[−3]
	2.10[−5]	1.28[−5]	8.54[−6]	4.71[−6]	2.68[−6]		2.06[−5]	3.26[−5]	4.38[−5]	6.26[−5]	8.03[−5]
6–20	1.11[−4]	1.26[−4]	1.39[−4]	1.59[−4]	1.75[−4]	9–16	1.17[−4]	1.12[−4]	1.14[−4]	1.24[−4]	1.37[−4]
	1.34[−4]	1.72[−4]	2.00[−4]	2.35[−4]	2.63[−4]		3.46[−6]	2.53[−6]	2.20[−6]	2.07[−6]	2.12[−6]
7–11	1.97[−5]	1.30[−5]	9.49[−6]	6.42[−6]	4.88[−6]	9–17	2.66[−5]	1.71[−5]	1.19[−5]	7.01[−6]	4.25[−6]
	0.0	0.0	0.0	0.0	0.0		1.51[−6]	8.60[−7]	5.53[−7]	2.97[−7]	1.67[−7]
7–12	7.61[−6]	4.51[−6]	2.93[−6]	1.51[−6]	7.98[−7]	9–18	5.92[−5]	4.10[−5]	3.16[−5]	2.31[−5]	1.88[−5]
	2.75[−7]	1.76[−7]	1.20[−7]	6.54[−8]	3.56[−8]		3.18[−6]	2.15[−6]	1.68[−6]	1.29[−6]	1.10[−6]
7–13	6.28[−5]	5.81[−5]	5.78[−5]	6.11[−5]	6.67[−5]	9–19	8.49[−5]	5.63[−5]	4.14[−5]	2.79[−5]	2.09[−5]
	6.09[−7]	6.87[−7]	7.56[−7]	8.71[−7]	9.80[−7]		3.50[−6]	1.99[−6]	1.28[−6]	6.86[−7]	3.86[−7]
7–14	8.31[−5]	9.75[−5]	1.09[−4]	1.28[−4]	1.45[−4]	9–20	1.45[−3]	1.51[−3]	1.54[−3]	1.58[−3]	1.61[−3]
	8.05[−7]	9.33[−7]	1.04[−6]	1.22[−6]	1.38[−6]		1.35[−4]	1.41[−4]	1.45[−4]	1.50[−4]	1.54[−4]
7–15	9.33[−5]	7.36[−5]	6.24[−5]	5.18[−5]	4.64[−5]	10–11	1.18[−5]	7.17[−6]	4.92[−6]	2.92[−6]	1.86[−6]
	1.51[−7]	1.65[−7]	1.79[−7]	2.02[−7]	2.26[−7]		4.24[−5]	2.64[−5]	1.82[−5]	1.07[−5]	6.45[−6]
7–16	2.14[−4]	2.47[−4]	2.79[−4]	3.29[−4]	3.79[−4]	10–12	5.84[−5]	6.35[−5]	6.66[−5]	7.00[−5]	7.23[−5]
	1.47[−6]	1.69[−6]	1.88[−6]	2.18[−6]	2.47[−6]		8.51[−4]	9.01[−4]	9.31[−4]	9.63[−4]	9.84[−4]
7–17	5.02[−5]	4.67[−5]	4.65[−5]	4.86[−5]	5.17[−5]	10–13	4.17[−5]	4.51[−5]	4.99[−5]	5.97[−5]	7.15[−5]
	0	0	0	0	0		1.20[−4]	1.54[−4]	1.87[−4]	2.43[−4]	3.00[−4]
7–18	3.77[−5]	2.54[−5]	1.91[−5]	1.37[−5]	1.11[−5]	10–14	7.51[−6]	5.15[−6]	3.71[−6]	2.23[−6]	1.35[−6]
	3.03[−8]	2.07[−8]	1.50[−8]	9.01[−9]	5.44[−9]		1.15[−5]	7.14[−6]	4.83[−6]	2.68[−6]	1.51[−6]
7–19	2.46[−5]	2.06[−5]	1.92[−5]	1.86[−5]	1.91[−5]	10–15	2.55[−5]	2.21[−5]	2.14[−5]	2.27[−5]	2.60[−5]
	0.0	0.0	0.0	0.0	0.0		6.25[−4]	9.34[−4]	1.21[−3]	1.63[−3]	2.06[−3]
7–20	6.94[−5]	4.43[−5]	3.08[−5]	1.81[−5]	1.11[−5]	10–16	3.51[−5]	2.39[−5]	1.71[−5]	1.02[−5]	6.12[−6]
	5.13[−6]	3.50[−6]	2.53[−6]	1.52[−6]	9.18[−7]		5.56[−5]	3.47[−5]	2.35[−5]	1.30[−5]	7.40[−6]
8–11	3.47[−5]	2.11[−5]	1.41[−5]	7.77[−6]	4.49[−6]	10–17	6.22[−5]	3.96[−5]	2.72[−5]	1.56[−5]	9.08[−6]
	2.47[−7]	1.31[−7]	8.08[−8]	4.12[−8]	2.24[−8]		6.16[−5]	3.78[−5]	2.54[−5]	1.41[−5]	8.03[−6]
8–12	3.82[−5]	4.12[−5]	4.43[−5]	4.92[−5]	5.36[−5]	10–18	1.08[−4]	7.00[−5]	4.96[−5]	3.04[−5]	1.99[−5]
	5.19[−6]	6.33[−6]	7.24[−6]	8.46[−6]	9.49[−6]		1.08[−4]	7.02[−5]	5.08[−5]	3.35[−5]	2.46[−5]
8–13	1.85[−4]	2.43[−4]	3.00[−4]	3.96[−4]	4.92[−4]	10–19	1.52[−4]	9.67[−5]	6.67[−5]	3.82[−5]	2.23[−5]
	7.61[−7]	7.66[−7]	8.86[−7]	1.18[−6]	1.49[−6]		1.43[−4]	8.75[−5]	5.87[−5]	3.25[−5]	1.85[−5]
8–14	6.79[−6]	4.00[−6]	2.63[−6]	1.40[−6]	7.76[−7]	10–20	7.35[−4]	9.32[−4]	1.07[−3]	1.26[−3]	1.40[−3]
	1.71[−7]	9.23[−8]	5.77[−8]	2.98[−8]	1.64[−8]		1.08[−3]	1.36[−3]	1.57[−3]	1.84[−3]	2.04[−3]
8–15	1.42[−4]	1.59[−4]	1.85[−4]	2.36[−4]	2.93[−4]	11–12	9.75[−4]	7.29[−4]	5.69[−4]	3.84[−4]	2.58[−4]
	8.67[−6]	1.33[−5]	1.76[−5]	2.48[−5]	3.17[−5]		9.94[−4]	7.43[−4]	5.78[−4]	3.90[−4]	2.61[−4]
8–16	3.48[−4]	3.92[−4]	4.36[−4]	5.08[−4]	5.81[−4]	11–13	1.49[+0]	1.65[+0]	1.68[+0]	1.72[+0]	1.77[+0]
	4.00[−6]	4.17[−6]	4.46[−6]	5.06[−6]	5.66[−6]		1.79[+0]	1.79[+0]	1.58[+0]	1.26[+0]	1.06[+0]

TABLE IV. (*Continued.*)

Transition	E_i (Ry)					Transition	E_i (Ry)				
$I-F$	85.0	127.5	170.0	250.0	350.0	$I-F$	85.0	127.5	170.0	250.0	350.0
11–14	7.81[−1]	8.63[−1]	8.82[−1]	8.99[−1]	9.26[−1]	14–15	1.22[−3]	7.58[−4]	5.17[−4]	2.94[−4]	1.72[−4]
	7.08[−1]	6.97[−1]	6.10[−1]	4.86[−1]	4.10[−1]		7.29[−4]	4.36[−4]	2.89[−4]	1.58[−4]	8.95[−5]
11–15	7.79[−1]	8.76[−1]	9.16[−1]	9.41[−1]	9.68[−1]	14–16	6.10[−2]	5.93[−2]	5.83[−2]	5.73[−2]	5.66[−2]
	2.28[−1]	2.30[−1]	2.23[−1]	1.88[−1]	1.56[−1]		1.49[−1]	7.58[−2]	6.72[−2]	6.24[−2]	6.02[−2]
11–16	3.60[+0]	4.04[+0]	4.24[+0]	4.37[+0]	4.50[+0]	14–17	1.11[+0]	1.14[+0]	1.14[+0]	1.17[+0]	1.21[+0]
	3.10[+0]	3.19[+0]	2.98[+0]	2.45[+0]	2.04[+0]		1.09[+0]	9.24[−1]	7.72[−1]	6.23[−1]	5.41[−1]
11–17	5.71[−2]	5.66[−2]	5.63[−2]	5.62[−2]	5.62[−2]	14–18	8.24[−4]	4.92[−4]	3.25[−4]	1.78[−4]	1.01[−4]
	6.06[−2]	5.81[−2]	5.74[−2]	5.74[−2]	5.78[−2]		8.35[−4]	4.95[−4]	3.25[−4]	1.76[−4]	9.90[−5]
11–18	9.47[−2]	9.40[−2]	9.35[−2]	9.33[−2]	9.32[−2]	14–19	7.01[−3]	7.44[−3]	7.77[−3]	8.25[−3]	8.65[−3]
	9.98[−2]	9.64[−2]	9.52[−2]	9.52[−2]	9.58[−2]		7.25[−3]	7.63[−3]	7.95[−3]	8.42[−3]	8.83[−3]
11–19	1.33[−1]	1.32[−1]	1.31[−1]	1.31[−1]	1.31[−1]	14–20	8.17[−4]	4.85[−4]	3.21[−4]	1.74[−4]	9.86[−5]
	1.40[−1]	1.36[−1]	1.34[−1]	1.34[−1]	1.35[−1]		8.22[−4]	4.84[−4]	3.18[−4]	1.71[−4]	9.56[−5]
11–20	2.58[−3]	1.72[−3]	1.29[−3]	9.10[−4]	7.13[−4]	15–16	5.91[−2]	5.50[−2]	5.31[−2]	5.11[−2]	4.98[−2]
	2.71[−3]	1.82[−3]	1.37[−3]	9.86[−4]	7.89[−4]		7.21[−2]	2.47[−2]	2.12[−2]	1.89[−2]	1.77[−2]
12–13	8.58[−1]	8.48[−1]	8.52[−1]	8.78[−1]	9.12[−1]	15–17	3.60[−1]	3.56[−1]	3.59[−1]	3.71[−1]	3.86[−1]
	3.04[−1]	2.26[−1]	1.88[−1]	1.57[−1]	1.39[−1]		9.27[−2]	6.89[−2]	5.93[−2]	5.13[−2]	4.62[−2]
12–14	1.84[−4]	1.18[−4]	8.28[−5]	4.88[−5]	2.92[−5]	15–18	8.42[−1]	8.37[−1]	8.45[−1]	8.74[−1]	9.09[−1]
	1.55[−4]	9.64[−5]	6.60[−5]	3.77[−5]	2.23[−5]		1.67[−1]	1.25[−1]	1.07[−1]	9.27[−2]	8.35[−2]
12–15	1.25[+0]	1.30[+0]	1.30[+0]	1.33[+0]	1.38[+0]	15–19	7.30[−3]	6.79[−3]	6.64[−3]	6.63[−3]	6.74[−3]
	2.04[+0]	1.85[+0]	1.56[+0]	1.24[+0]	1.06[+0]		4.59[−3]	3.51[−3]	3.02[−3]	2.63[−3]	2.48[−3]
12–16	8.82[−4]	5.61[−4]	3.91[−4]	2.28[−4]	1.37[−4]	15–20	1.96[+0]	2.15[+0]	2.21[+0]	2.26[+0]	2.33[+0]
	7.79[−4]	4.83[−4]	3.30[−4]	1.89[−4]	1.11[−4]		2.67[+0]	2.47[+0]	2.12[+0]	1.71[+0]	1.47[+0]
12–17	4.13[−4]	2.45[−4]	1.61[−4]	8.69[−5]	4.85[−5]	16–17	7.23[−2]	7.24[−2]	7.36[−2]	7.66[−2]	7.98[−2]
	4.25[−4]	2.51[−4]	1.65[−4]	8.82[−5]	4.91[−5]		6.63[−2]	5.38[−2]	4.80[−2]	4.35[−2]	4.10[−2]
12–18	1.10[−3]	8.19[−4]	6.80[−4]	5.59[−4]	4.95[−4]	16–18	8.99[−1]	8.95[−1]	9.06[−1]	9.40[−1]	9.78[−1]
	1.21[−3]	9.04[−4]	7.61[−4]	6.41[−4]	5.78[−4]		7.87[−1]	6.03[−1]	5.11[−1]	4.32[−1]	3.86[−1]
12–19	9.64[−4]	5..71[−4]	3.75[−4]	2.01[−4]	1.12[−4]	16–19	5.00[+0]	5.01[+0]	5.07[+0]	5.25[+0]	5.47[+0]
	9.95[−4]	5.88[−4]	3.84[−4]	2.06[−4]	1.14[−4]		4.26[+0]	3.31[+0]	2.79[+0]	2.33[+0]	2.06[+0]
12–20	9.39[−2]	9.37[−2]	9.35[−2]	9.35[−2]	9.36[−2]	16–20	6.25[−3]	4.89[−3]	4.16[−3]	3.52[−3]	3.25[−3]
	9.82[−2]	9.47[−2]	9.37[−2]	9.40[−2]	9.47[−2]		7.67[−3]	6.04[−3]	4.83[−3]	3.52[−3]	2.77[−3]
13–14	3.17[−3]	2.20[−3]	1.63[−3]	1.03[−3]	6.58[−4]	17–18	6.28[−2]	5.79[−2]	5.55[−2]	5.31[−2]	5.17[−2]
	3.76[−3]	2.58[−3]	1.90[−3]	1.19[−3]	7.51[−4]		1.26[+0]	6.97[−2]	6.13[−2]	5.63[−2]	5.39[−2]
13–15	9.31[−2]	9.00[−2]	8.84[−2]	8.68[−2]	8.57[−2]	17–19	1.32[−2]	1.23[−2]	1.21[−2]	1.21[−2]	1.23[−2]
	6.62[−2]	5.26[−2]	4.81[−2]	4.50[−2]	4.34[−2]		2.52[−2]	1.37[−2]	1.30[−2]	1.27[−2]	1.28[−2]
13–16	8.75[−2]	8.41[−2]	8.23[−2]	8.04[−2]	7.91[−2]	17–20	4.70[−3]	2.85[−3]	1.96[−3]	1.18[−3]	7.85[−4]
	3.08[−1]	1.50[−1]	1.34[−1]	1.24[−1]	1.19[−1]		4.95[−3]	3.00[−3]	2.06[−3]	1.24[−3]	8.25[−4]
13–17	4.89[−1]	5.01[−1]	5.04[−1]	5.16[−1]	5.35[−1]	18–19	7.68[−2]	7.12[−2]	6.85[−2]	6.61[−2]	6.48[−2]
	7.10[−1]	5.88[−1]	4.90[−1]	3.98[−1]	3.47[−1]		1.40[−1]	8.19[−2]	7.46[−2]	6.98[−2]	6.75[−2]
13–18	1.72[+0]	1.78[+0]	1.79[+0]	1.84[+0]	1.90[+0]	18–20	7.75[−3]	4.70[−3]	3.21[−3]	3.77[−3]	1.39[−3]
	2.18[+0]	1.84[+0]	1.54[+0]	1.25[+0]	1.09[+0]		8.93[−3]	5.18[−3]	3.41[−3]	2.02[−3]	1.30[−3]
13–19	1.10[−2]	1.06[−2]	1.06[−2]	1.08[−2]	1.11[−2]	19–20	1.10[−2]	6.69[−3]	4.57[−3]	2.69[−3]	1.70[−3]
	1.44[−2]	1.44[−2]	1.46[−2]	1.52[−2]	1.57[−2]		1.15[−2]	7.01[−3]	4.79[−3]	2.84[−3]	1.81[−3]
13–20	8.77[−1]	9.84[−1]	1.03[+0]	1.06[+0]	1.09[+0]						
	2.10[−1]	2.15[−1]	2.01[−1]	1.67[−1]	1.41[−1]						

namical part. Very accurate atomic structure calculated by multiconfiguration Dirac-Fock theory is used in these calculations. The collision strengths for both resonance transitions and transitions between excited levels by 133-level MCDF CE and 20-level MCDF CE are tabulated. Good agreements are found between the two calculation modes for transitions between low-energy levels. However, very large differences are found if one of the transition levels is high. Hence, in such cases it is necessary to use 133-level MCDF CE to obtain these collision strengths. The collision strengths for transitions from excited levels in $2p^2$ or $2s3l$ ($l=s,p,d$) to excited levels in $2s3l$ ($l=s,p,d$) calculated by 133-level MCDF CE are presented for the first time, to the best of our knowledge.

The present results have been comprehensively compared with other calculations. Significant differences have been found. For some transitions, even the qualitative trends of the collision strengths versus electron impact energies are quite

different between our calculations and the others. The reason for the difference for resonance transition to $2s2p\ ^3P_1$ between DW or RDW calculations and R-matrix or Dirac R-matrix calculations, which was often discussed, is attributed both to insufficient partial waves used in the R-matrix calculations and to channel coupling being ignored in the DW or RDW calculations. We have established that the influence of the channel coupling on the difference for this transition is not the only cause. The collision strengths for transitions between levels that have strong configuration interaction effects such as levels 13–16 with odd parity are especially sensitive to the calculation models. Therefore, in order to obtain highly accurate collision strengths, it is necessary to include properly the correlation effect and relativistic effect as well as higher-order relativistic effects in the calculation model.

Because our collision strengths are obtained by RDW method and more correlation and relativistic effects than before are caught by 133-level MCDF configuration expansion, they should be more accurate and reliable. Hence, these new collision strengths should enable a reexamination of the Fe XXIII lines expected in laboratory experiments or solar flare spectra and related plasmas modeling and diagnostics.

ACKNOWLEDGMENTS

The authors are indebted to Professor I. P. Grant and Dr. P. Marketos for providing us with the GRASP[2] code. We are also grateful to the National Supercomputing Research Center (NSRC) of Singapore for professional advice on and use of their Cray T94 supercomputer.

[1] G. E. Bromage, R. D. Cowan, B. C. Fawcett, and A. Ridgeley, J. Opt. Soc. Am. **68**, 48 (1978).
[2] K. D. Lawson and N. J. Peacock, Astron. Astrophys., Suppl. Ser. **58**, 475 (1984).
[3] Guo-xin Chen and P. P. Ong, this issue, Phys. Rev. A **58**, 1070 (1998).
[4] C. Møller, Ann. Phys. (Leipzig) **14**, 531 (1932).
[5] P. H. Norrington and I. P. Grant, J. Phys. B **20**, 4869 (1987).
[6] F. P. Keenan, E. S. Conlon, G. A. Warren, A. W. Boone, and P. H. Norrington, Astrophys. J. **406**, 350 (1993).
[7] N. S. Scott and P. G. Burke, J. Phys. B **13**, 4299 (1980).
[8] H. L. Zhang and D. H. Sampson, At. Data Nucl. Data Tables **52**, 143 (1992).
[9] H. L. Zhang and D. H. Sampson, Phys. Rev. A **47**, 208 (1993).
[10] W. J. Qian, Y. K. Kim, and J. P. Desclaux, Phys. Rev. A **39**, 4509 (1989).
[11] D. H. Sampson, R. E. H. Clark, and S. J. Goett, Phys. Rev. A **24**, 2979 (1981).
[12] W. Eissner, M. Jones, and H. Nussbaumer, Comput. Phys. Commun. **8**, 271 (1974).
[13] W. Eissner and M. J. Seaton, J. Phys. B **5**, 2187 (1972).
[14] H. E. Saraph, Comput. Phys. Commun. **3**, 256 (1972).
[15] A. K. Bhatia and H. E. Mason, Astron. Astrophys. **103**, 324 (1981).
[16] A. K. Bhatia and H. E. Mason, Astron. Astrophys. **155**, 413 (1986).
[17] Guo-xin Chen, Phys. Rev. A **53**, 3227 (1996); **56**, 3765 (1997).
[18] GRASP[2], F. A. Parpia, I. P. Grant, and C. F. Fischer (unpublished).
[19] K. G. Dyall, I. P. Grant, C. T. Johnson, F. A. Parpia, and E. P. Plummer, Comput. Phys. Commun. **55**, 425 (1989), and references therein.
[20] Guo-xin Chen and P. P. Ong, Phys. Rev. A **57**, 4991 (1998).